ACS OMEGA

http://pubs.acs.org/journal/acsodf

Article

Designing $CoS_{1.035}$ Nanoparticles Anchored on N-Doped Carbon Dodecahedron as Dual-Enzyme Mimics for the Colorimetric Detection of H_2O_2 and Glutathione

Tao Chen,[§] Yuanhong Min,[§] Xiao Yang, Hao Gong, Xiaoying Tian, Li Liu,* Yanhua Hou,* and Wensheng Fu*

Cite This: *ACS Omega* 2022, 7, 11135−11147

Read Online

ACCESS | Metrics & More | Article Recommendations | Supporting Information

ABSTRACT: In recent years, the exploration of the nanozyme, an artificial enzyme with the structure and function of natural enzymes, has become a hot topic in this field. Although significant progress has been made, it is still a huge challenge to design nanozymes with multiple enzyme-like catalytic activities. In this work, we have successfully fabricated a colorimetric sensing platform to mimic peroxidase-like and oxidase-like activities by the $CoS_{1.035}$ nanoparticles decorated N-doped carbon framework porous dodecahedrons (abbreviated to $CoS_{1.035}$/N-C PDHs). And the catalytic mechanism of $CoS_{1.035}$/N-C PDHs toward the peroxidase-like and oxidase-like activities is systematically explored. The results display that $CoS_{1.035}$/N-C PDHs can catalyze the oxidation of the colorless substrate 3,3′,5,5′-tetramethylbenzidine (TMB) into blue oxidized TMB (ox-TMB) by disintegrating H_2O_2 or the physically/chemically absorbed O_2 into different ROS species (·OH or $O_2^{\cdot-}$) in the presence or absence of H_2O_2. Therefore, on the basis of the dual-enzyme mimic activities of $CoS_{1.035}$/N-C PDHs, the bifunctional colorimetric sensing platform is established for H_2O_2 detection with a wide linear range of 0.5−120 μM and glutathione detection with a linear range of 1−60 μM, respectively. This work provides an efficient platform for dual-enzyme mimics, expanding the application prospect of Co-based chalcogenides as enzyme mimics in biosensing, medical diagnosis, and environment monitoring.

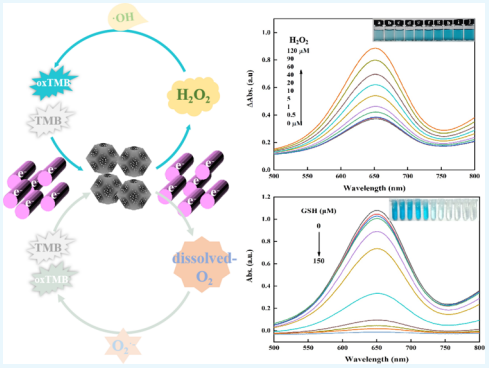

1. INTRODUCTION

Most natural enzymes, as powerful biocatalysts, are a class of biological macromolecules (a few are RNAs) with high selectivity and catalytic activity, which play a substantial role in many biological processes. However, owing to the difficulty of preparation, high cost, poor stability, and other inherent defects, their application is seriously hindered.[1,2] In the last 10 years, as novel artificial enzymes, nanozymes have been developed to substitute natural enzymes.[3] They are defined as nanomaterials with enzyme-like properties (which can simulate the structure and function of enzymes).[4,5] Since magnetic Fe_3O_4 nanoparticles were first proven to show intrinsic peroxidase-like properties in 2007,[6] a surge of inorganic nanomaterials has been found to possess enzyme-like properties, such as noble metals,[7] metal oxides[8] and sulfides,[9−11] carbon materials,[12] and metal organic frameworks and their derivatives.[13,14] Due to the diverse structure, easy surface modification, adjustable activity, large surface area, simple preparation, low cost, and high stability (tolerance to strong acid and alkali and resistance to high temperature), nanozymes have broad application prospects in the fields of chemical sensing, biological analysis, medical diagnosis, and environmental conservation.[15−18] However, compared with natural enzymes, nanozymes have no substrate specificity, and their catalytic activity is still low.[19] Moreover, generally, most nanozymes only display one characteristic enzyme-like catalytic activity, which restrains their further application in the fields of analysis, sensing, and others. Thus, it is a huge challenge to design highly efficient nanozymes with multiple enzymatic mimetic properties, which exhibit promising applications for colorimetric sensing.

Recently, transition metal chalcogenides (TMCs) were reported to own intrinsic enzyme-like catalytic properties.[20,21] For example, Xia *et al.*[22] reported that the MoS_2 quantum dot possesses excellent peroxidase-like activity through precisely controlling the existence form of the MoS_2 quantum dot with the help of Fe^{3+} ions. Based on the finding, they established a reliable colorimetric detection platform for pyrophosphate. Besides, He *et al.*[23] prepared a CuS concave polyhedral superstructure through a green solvothermal reaction, which

Received: December 23, 2021
Accepted: March 1, 2022
Published: March 24, 2022

https://doi.org/10.1021/acsomega.1c07264
ACS Omega 2022, 7, 11135−11147

Scheme 1. Schematic Presentation of the Synthesis Procedure of Co_xM/N-C PDHs (M = O, S, Se, Te)

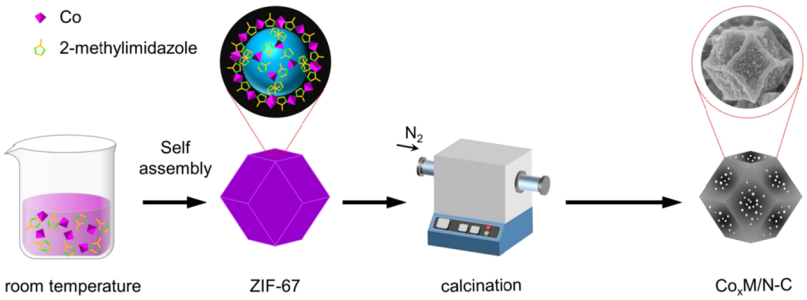

exhibits intrinsic peroxidase-like activity, as it can catalyze TMB and OPD oxidation quickly in the presence of hydrogen peroxide. Likewise, Wang *et al.*[24] synthesized the hollow CuS nanocube, which also displays outstanding peroxidase-like property. And they found that the excellent catalysis property is attributed to the existence of copper, endowing the hollow CuS nanocube with the characteristics of Fenton's reagents. On the basis of the research of Wang *et al.*, Song *et al.*[9] designed FeS_2 nanoparticles as peroxidase mimicase owing to their suitable band gap and extraordinary absorption coefficient. And then, a sensitive colorimetric method for H_2O_2 and glutathione (GSH) detection was developed. Considering the similar electron structure of Fe, Cu, and Co, we reasonably speculate that the cobaltous sulfides might also hold a great potential to be a mimic enzyme. Although some progress has been made in this field,[25] the exploration of cobaltous sulfides as dual-enzyme mimics and the subsequent application in colorimetric sensing are still in their infancy. Therefore, it is of great significance to develop a bifunctional nanozyme with excellent enzyme-like activity and stability.

Based on the above-mentioned condition, in this work, we designed $CoS_{1.035}$/N-C porous dodecahedrons (PDHs) as bifunctional mimic enzymes, in which $CoS_{1.035}$ nanoparticles are uniformly dispersed on a porous N-doped carbon dodecahedron framework. The $CoS_{1.035}$/N-C PDH nanozyme owns multiple advantages, such as the fact that the dodecahedron carbon framework offers abundant channels for electrons, facilitating electron transfer from the catalyst to reactant, and the porous property brings about a huge surface area to promote the fast contact of substrates with the catalytically active sites. Besides, N atoms dope into the carbon framework, which alter the surface charge property of the $CoS_{1.035}$/N-C PDH nanozyme catalyst. In addition, the $CoS_{1.035}$ nanoparticles are anchored on the N-doped carbon dodecahedron framework, which could prevent the active nanoparticles from being directly exposed to the reaction solution. All of the above endow the $CoS_{1.035}$/N-C PDH nanozyme catalyst with glorious dual-enzyme mimic activities and stability. As a result, $CoS_{1.035}$/N-C PDHs exhibit satisfactory peroxidase-like and oxidase-like activities, which could catalyze the oxidation of the colorless substrate 3,3′,5,5′-tetramethylbenzidine (TMB) into blue oxidized TMB (ox-TMB) in either the presence or absence of H_2O_2. Consequently, combined with the inoxidizability of glutathione (GSH), a bifunctional colorimetric sensing platform for the visual detection of H_2O_2 and GSH was designed. The proposed method shows great potential application in clinical diagnosis, environmental protection, and the food industry.

2. RESULTS AND DISCUSSION

2.1. Synthesis and Characterization of Co_xM/N-C (M = O, S, Se, Te) PDHs. As shown in Scheme 1, first, the precursor ZIF-67 nanomaterial was prepared by self-assembly of cobalt nitrate and dimethyl imidazole at room temperature, and then the Co/N-C intermediate was obtained by annealing the as-prepared ZIF-67 dodecahedron under a N_2 flow atmosphere. During this process, the nitrogenous organic ligands were carbonized to form porous N-doped carbon framework dodecahedrons, while the Co^{2+} ions were reduced to Co nanoparticles by the derived carbon. Finally, the Co_xM/N-C porous dodecahedrons (marked as Co_xM/N-C PDHs) with the morphology of the precursor were fabricated by introduction of the chalcogen element (M = O, S, Se, Te) through high heat treatment.

To explore the structural feature and stability of the synthesized ZIF-67 precursor, field emission scanning electron microscope (FE-SEM), X-ray diffraction (XRD), and thermogravimetry (TG) analysis were carried out. As shown in Figures S1a and S3a,e, the as-obtained ZIF-67 precursor exhibits the morphology of a typical rhombic dodecahedron with an average size of 751.9 ± 7.2 nm (Figure S1b). And the XRD pattern (Figure S1c) shows that the ZIF-67 dodecahedron has good crystallinity even without high heat treatment, suggesting the high thermal stability. The high thermal stability makes the ZIF-67 dodecahedron an ideal carbon-based precursor to maintain its initial porous morphology and avoid excessive vaporization during the annealing process. Thermogravimetry analysis in Figure S1d displays that the weight loss (4.67%) of the ZIF-67 dodecahedron below 550 °C is attributed to the removal of solvents and dehydration. When the temperature is elevated from 550 to 600 °C, the nitrogenous organic ligand is totally decomposed to form a N-doped carbon framework causing a significant weight loss (31.54%). In this process, a large number of pores are produced due to the decomposition of organic linkers. Meanwhile, Co^{2+} ions are reduced to Co nanoparticles by the derived carbon, inducing the transformation from the ZIF-67 precursor into the Co/N-C intermediate. When the temperature is above 600 °C, there is a degree of weight loss probably due to the structural collapse of the N-doped carbon framework. These results show that when the annealed temperature is above 550 °C, the pure Co/N-C intermediate can be successfully obtained. Therefore, three Co/N-C intermediates under different annealed temperatures (550, 600, and 700 °C) were prepared. Figure S2 reveals that the XRD diffraction peaks of the three samples are consistent with the cubic Co phase (JCPDS no. 89-4307) without a sign of the precursor, indicating that the ZIF-67 precursor transforms into the Co/N-C intermediate successfully. As shown in Figure S3b,f, the Co/N-C intermediate (550

https://doi.org/10.1021/acsomega.1c07264
ACS Omega 2022, 7, 11135−11147

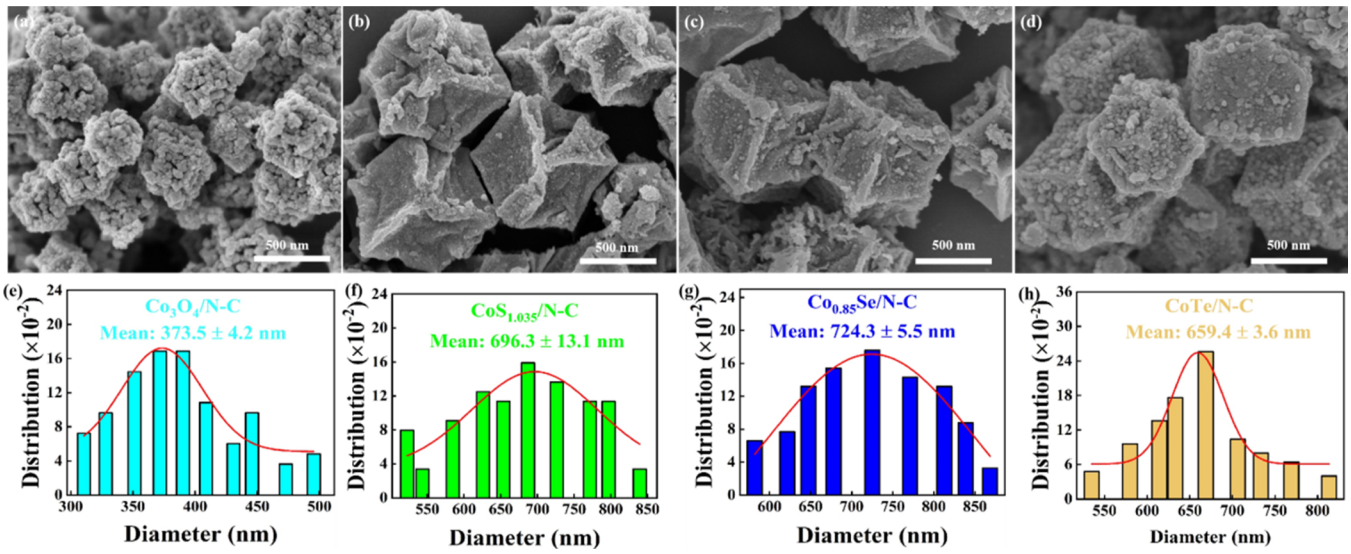

Figure 1. The SEM images and size distributions of Co_xM/N-C PDHs (M = O, S, Se, Te). (a, e) Co_3O_4/N-C; (b, f) $CoS_{1.035}$/N-C; (c, g) $Co_{0.85}Se$/N-C; and (d, h) CoTe/N-C.

°C) perfectly inherits the dodecahedron morphology of the ZIF-67 precursor, but the active Co nanoparticles have not been formed obviously. When carbonized at 600 °C, the Co/N-C (600 °C) dodecahedron with a slightly sunken surface can be obtained, and Co nanoparticles with a small size are evenly distributed on the N-doped carbon framework (Figure S3c,g). At 700 °C, the N-doped carbon framework of the Co/N-C (700 °C) dodecahedron collapses slightly, and Co nanoparticles increase in size due to agglomeration (Figure S3d,h). It can be seen that the annealing temperature can affect the collapsed degree of the N-doped carbon framework and the size of Co nanoparticles, which may further affect the catalytic activity of the subsequently synthesized Co_xM/N-C (M = O, S, Se, Te) PDHs. Therefore, we compared the catalytic performance of the above three intermediates, as shown in Figure S4. It is not difficult to find that the as-prepared Co/N-C (600 °C) exhibits the highest catalytic activity among the three intermediates, which may be attributed to the smaller size and uniform distribution of the active centers on the N-doped carbon framework. After comprehensive consideration, the Co/N-C (600 °C) intermediate was selected for subsequent research.

To better regulate the catalytic performance, Co_xM/N-C (M = O, S, Se, Te) PDHs with a concave surface were synthesized and characterized. Figure 1 shows the SEM images of Co_xM/N-C (M = O, S, Se, Te) PDHs. It can be seen that except for Co_3O_4/N-C PDHs, other samples, such as Co_xM/N-C (M = S, Se, Te) PDHs, keep the concave dodecahedron morphology. The Co_3O_4/N-C nanostructure is composed of small particles as building blocks. Its morphology collapses completely probably due to the destruction of the carbon framework during calcination in the air. In addition, the sizes of Co_xM/N-C (M = O, S, Se, Te) PDHs are 373.5 ± 4.2 nm (Co_3O_4/N-C), 696.3 ± 13.1 nm ($CoS_{1.035}$/N-C), 724.3 ± 5.5 nm ($Co_{0.85}Se$/N-C), and 659.4 ± 3.6 nm (CoTe/N-C), respectively, which are smaller than those of ZIF-67. The results show that the diameter of Co_xM/N-C (M = O, S, Se, Te) PDHs decreases after heat treatment. Figure S5 exhibits the XRD patterns of the obtained Co_xM/N-C (M = O, S, Se, Te) PDHs. The diffraction peaks of all samples match well with the corresponding standard cards, indicating the acquisition of pure phases. Besides, element mapping analysis was used to measure the percentages of each element in the Co_xM/N-C (M = O, S, Se, Te) PDHs and intermediate Co/N-C PDHs, as displayed in Table S1, which indirectly proves the successful synthesis of the above materials. More convincing evidence is offered by the inductive coupled plasma atomic emission spectrometer (ICP-AES) in Table S2, in which the Co/M mole ratios are well consistent with the results in XRD. Figure S6 displays the uniform distribution of C, N, Co, and the chalcogen element (M = O, S, Se, Te) over the entire architecture of porous dodecahedrons. The above observations prove the successful synthesis of four Co_xM/N-C (M = O, S, Se, Te) PDHs. Then, we compared their catalytic performance as exhibited in Figure S7. Obviously, among these nanomaterials, $CoS_{1.035}$/N-C PDHs exhibit the best peroxidase-like activity. As is well known, the performance of catalysts is mainly determined by their composition, structure, and morphology. As shown in Figure S6b−e, four Co_xM/N-C (M = O, S, Se, Te) materials have similar morphology with porous dodecahedrons (PDHs). The difference is that the structure of Co_3O_4/N-C PDHs has completely collapsed owing to the destruction of the carbon framework during calcination in the air. This reason may be attributed to the suboptimal performance of Co_3O_4/N-C PDHs. Besides, an ideal peroxidase- and oxidase-like catalyst should serve as the electron acceptor, which could receive the electrons from reactants. In three Co_xM/N-C (M = S, Se, Te) PDHs, tellurides have typical metallic properties; thus, its ability to gain electrons is limited. And sulfur is more electronegative than selenium; consequently, $CoS_{1.035}$/N-C PDHs own higher peroxidase- and oxidase-like activities. To explore the intrinsic factor of the enhanced activity, more elaborate characterizations toward $CoS_{1.035}$/N-C PDHs were carried out.

Figure 2 shows the scanning electron microscope (SEM) images, transmission electron microscope (TEM) images, and high-resolution transmitting electron microscope (HRTEM) images of $CoS_{1.035}$/N-C PDHs. In Figure 2a,c, the large-scale $CoS_{1.035}$/N-C PDHs with a uniform size can be observed. They inherit the porous dodecahedron morphology of intermediate Co/N-C PDHs perfectly, suggesting the excellent structural stability. And a large number of $CoS_{1.035}$ nanoparticles are

https://doi.org/10.1021/acsomega.1c07264
ACS Omega 2022, 7, 11135−11147

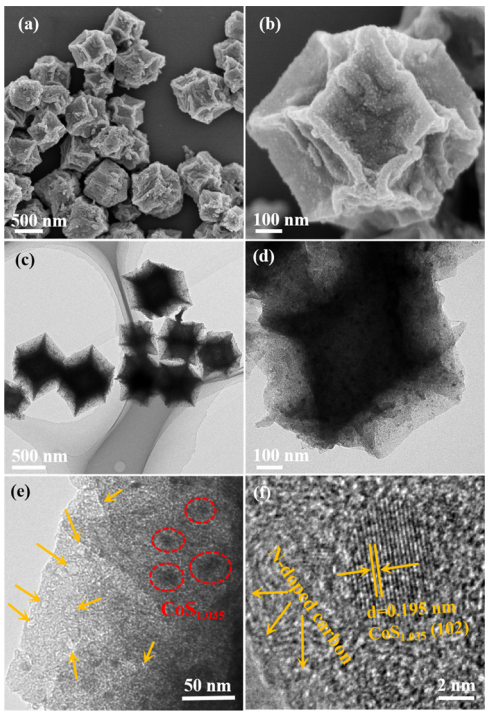

Figure 2. (a, b) The SEM images, (c, d) TEM images, and (g) HRTEM images of $CoS_{1.035}$/N-C PDHs.

evenly distributed on the N-doped carbon dodecahedron framework, as shown in Figure 2b,d. No significant agglomeration has been discovered. Further observation (Figure 2e) reveals that the size of $CoS_{1.035}$ nanoparticles falls in the range of 15−30 nm, as indicated by the red circles. Notably, some light and shade contrasts (as indicated by the yellow arrows) can be discerned in the enlarged TEM image (Figure 2e), implying the presence of abundant pores. Thus, the nitrogen adsorption−desorption isotherm was investigated to prove the porous structure. As exhibited in Figure S8, $CoS_{1.035}$/N-C PDHs display a combination of type-I and type-IV isotherm characteristics with an additional H_4-type broad hysteresis loop at p/p_0 = 0.5−0.99, revealing the existence of a mesoporous structure in $CoS_{1.035}$/N-C PDHs. The pore-size distribution of $CoS_{1.035}$/N-C PDHs mainly focuses on 3.89 nm. Such porous structure brings about a high surface area (230.692 $m^2\ g^{-1}$). This intriguing structure is believed to be advantageous for the exposure of active sites and mass transport of the substrates. Besides, the HRTEM image in Figure 2f reveals a set of regular lattice fringes with an interplanar crystal distance of 0.195 nm corresponding to the (102) lattice plane of $CoS_{1.035}$, which is consistent with the XRD results.

To further investigate the surface chemical components and chemical states of the $CoS_{1.035}$/N-C PDHs, X-ray photoelectron spectroscopy (XPS) measurement was performed. The binding energies of all spectra are calibrated strictly using the standard C 1s peak (284.8 eV). As shown in Figure 3a, the XPS survey spectrum of $CoS_{1.035}$/N-C PDHs exhibits the presence of C, N, O, S, and Co elements, wherein the O element is derived from the surface oxidation (531.1 eV), dissociative oxygen (532.0 eV), and adsorbed oxygen (533.4 eV), which is proven by the O 1s XPS spectrum (Figure 3b). And Figure 3c−f exhibits, respectively, XPS spectra of the C 1s, N 1s, S 2p, and Co 2p region for the samples. The asymmetrical C 1s peak in Figure 3c is composed of three independent peaks, which could be assigned to COO^- (288.5 eV),C═N (285.8 eV), and C═C (284.8 eV), respectively.[26]

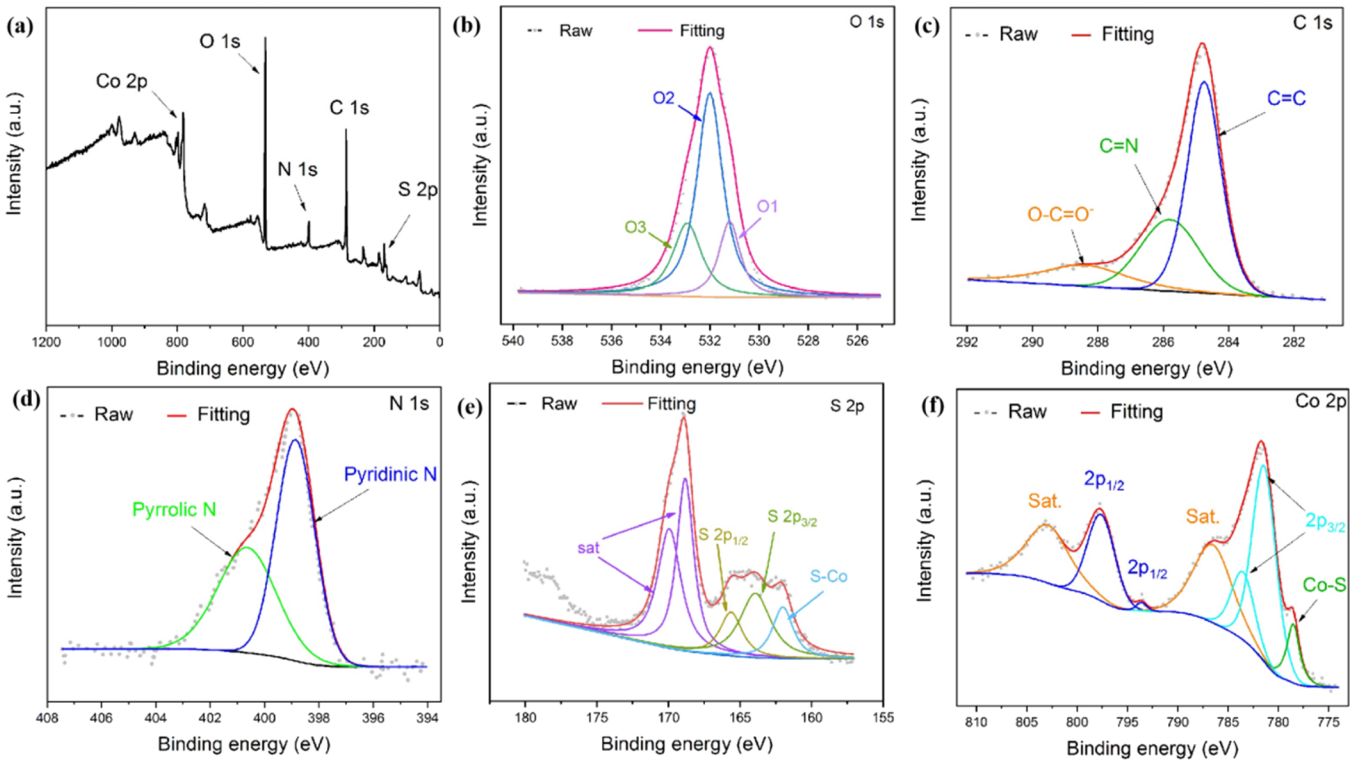

Figure 3. (a) The survey scan of $CoS_{1.035}$/N-C. The high-resolution XPS spectra of (b) O 1s, (c) C 1s, (d) N 1s, (e) S 2p, and (f) Co 2p in the $CoS_{1.035}$/N-C PDHs, respectively.

https://doi.org/10.1021/acsomega.1c07264
ACS Omega 2022, 7, 11135−11147

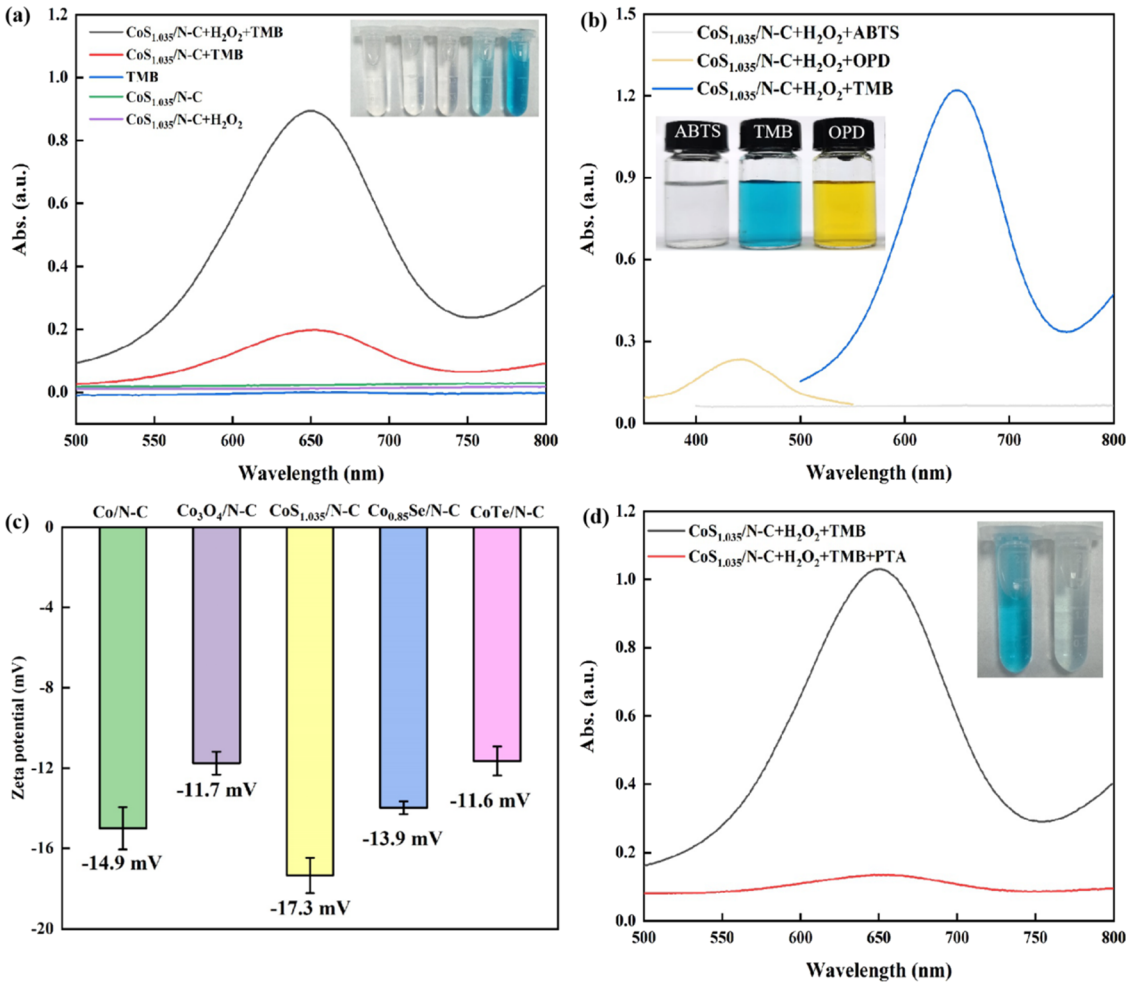

Figure 4. (a) The UV−vis absorption spectra of different test systems in the absence and presence of 20 mM H_2O_2, 15 μg/mL $CoS_{1.035}$/N-C PDHs, and 50 μg/mL TMB. (b) The UV−vis absorption spectra of 15 μg/mL $CoS_{1.035}$/N-C PDHs with 20 mM H_2O_2 in the different substrates (50 μg/mL). (c) The zeta potential measurements of Co/N-C and Co_xM/N-C PDHs (M = O, S, Se, Te). The error bars represent the standard deviation values of three measurements. (d) The UV−vis absorption spectra of 15 μg/mL $CoS_{1.035}$/N-C PDHs, 20 mM H_2O_2, and 50 μg/mL TMB in the absence or presence PTA.

For the N 1s region (Figure 3d), the original peak is deconvoluted into four peaks, that is, graphitic N (400.7 eV), pyrrolic N (399.5 eV), Co−N (399.1 eV), and pyridinic N (398.7 eV).[27] The graphitic N atoms are inserted into the carbon layer and bond to three adjacent carbon atoms, which may have a p-doping effect on the N-doped carbon, while the pyrrolic N and pyridinic N atoms increase the density of the electronic states of carbon and open the band gap,[27] altering the surface charge property. Consequently, it facilitates the electron transfer from the catalyst to reactant, contributing to the prominent catalytic activity. In the S 2p region, as shown in Figure 3e, the binding energies of two satellites, S $2p_{1/2}$, S $2p_{3/2}$, and S-Co species are observed at 170.1, 168.9, 165.5, 164.0, and 162.1 eV, respectively.[28,29] For the Co 2p region, as illustrated in Figure 3f, it could be resolved into seven peaks, involving satellites (at 803.1 and 786.7 eV), Co $2p_{1/2}$ (at 797.7 and 793.6 eV), Co $2p_{3/2}$ (at 783.7 and 781.5 eV), and the Co−S bond (at 778.5 eV). The peaks located at 781.5 and 778.5 eV are attributed to the Co−N_x and Co−S species, respectively. These observations confirm the existence of Co^{2+}/Co^{3+} ions on the surface of $CoS_{1.035}$/N-C PDHs.[28,30] The above results show that the $CoS_{1.035}$/N-C PDHs were successfully prepared, which are in accord with the XRD and HRTEM analysis. Additionally, Raman measurement is an efficient tool to detect the structural properties of carbon-based materials. The Raman spectrum in Figure S9 reveals two characteristic peaks of the D band (1347 cm^{-1}) and G band (1588 cm^{-1}) of carbon materials. The D band reflects the disordered carbon or defective graphitic structures resulting from edge doping of N atoms in the carbon framework. The G band represents the existence of the graphitic structure.[31] The I_D/I_G value of 1.17 implies the presence of a large number of defects in the N-doped carbon framework. These defects are in favor of accelerating the interfacial electron transfer between the catalyst and substrates, which could partially account for the excellent catalytic activity of $CoS_{1.035}$/N-C PDHs.

2.2. Exploring the Peroxidase-Like Activity of $CoS_{1.035}$/N-C PDHs. Considering the structural advantages, such as the hollow dodecahedron morphology with a huge surface area, stable N-doped carbon framework, and ultrafine $CoS_{1.035}$ nanoparticles, the $CoS_{1.035}$/N-C PDH material is deemed as a promising enzyme mimic catalyst. Therefore, the catalytic activities of the $CoS_{1.035}$/N-C PDHs were investigated by performing the peroxidase-mediated oxidation reactions of 3,3′,5,5′-tetramethylbenzidine (TMB) in the presence of H_2O_2. As demonstrated in Figure 4a, $CoS_{1.035}$/N-C PDHs

https://doi.org/10.1021/acsomega.1c07264
ACS Omega 2022, 7, 11135−11147

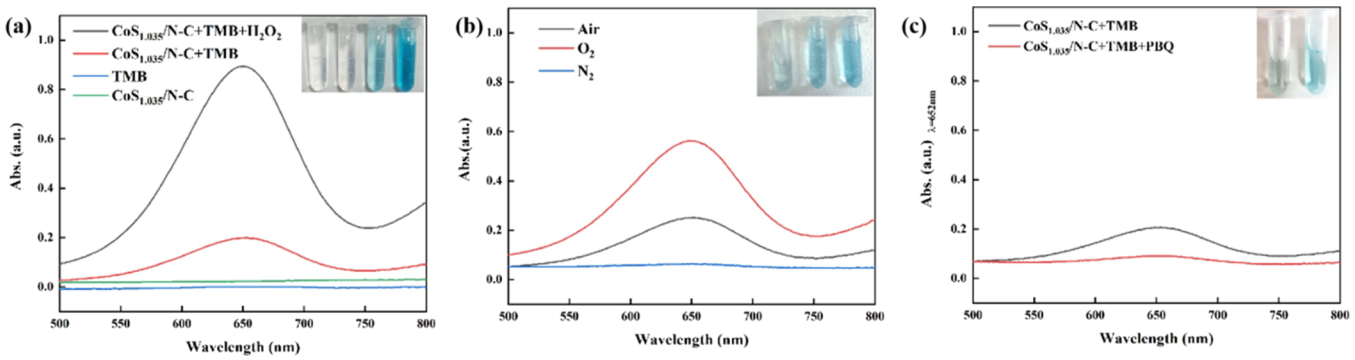

Figure 5. (a) The UV−vis absorption spectra of various reaction systems in an acetate buffer solution (pH = 5.0). (b) The UV−vis absorption spectra of reaction systems in air-saturated, O_2-saturated, and N_2-saturated systems. The reaction system consists of TMB (50 μg/mL), $CoS_{1.035}$/N-C PDHs (15 μg/mL), H_2O_2 (10 mM) in HAc-NaAc buffer solution (pH = 5.0). (c) The UV−vis absorption spectra of 15 μg/mL $CoS_{1.035}$/N-C PDHs and 50 μg/mL TMB in the absence or presence PBQ. The inset is the corresponding photograph.

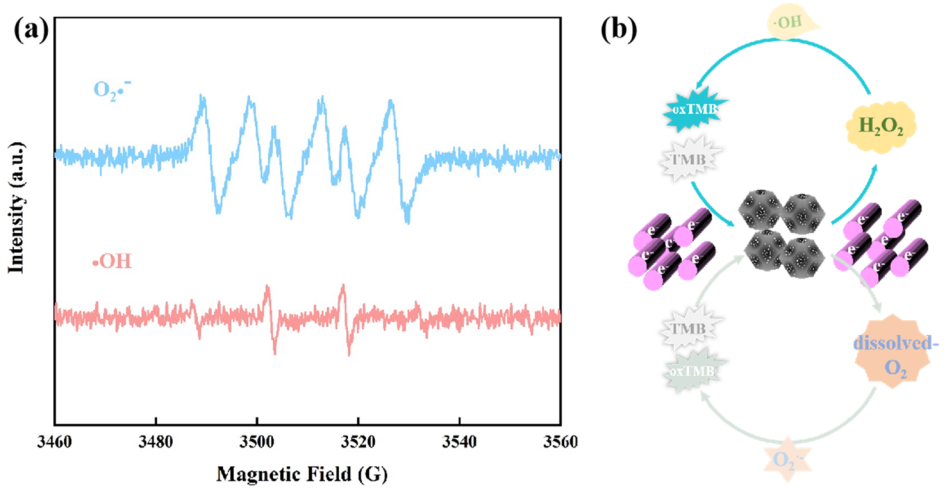

Figure 6. (a) The typical EPR spectrum: ·OH and $O_2{\cdot}^-$ originated from the $CoS_{1.035}$/N-C PDHs +H_2O_2+ DMPO system. (b) The proposed reaction mechanism of dual-enzyme mimic activities for $CoS_{1.035}$/N-C PDHs.

could catalyze the oxidation of TMB by H_2O_2 to generate the typical blue color and an absorption peak at 652 nm, which could be applied as a colorimetric probe to oxTMB. In contrast, the individual $CoS_{1.035}$/N-C + H_2O_2 or TMB + H_2O_2 system does not display the obvious colorimetric response and absorbance, implying the outstanding peroxidase-like activity of $CoS_{1.035}$/N-C PDHs. More distinct phenomenon exhibits in the time-course profile (Figure S10a). The intensity of the absorption peak gradually rises and the color of the test solution becomes darker as time goes on. Besides, the responses of absorbance are particularly rapid accompanied with the concentration increases of TMB and H_2O_2, as shown in Figure S10b,c, proving the fast reaction rate.

To prove the specificity of $CoS_{1.035}$/N-C PDHs toward substrates, reaction systems with different chromogenic substrates, such as TMB, OPD, and ABTs, were also employed for comparison. By visual inspection and spectral measurements, the chromogenic substrates TMB and OPD could be catalyzed by the $CoS_{1.035}$/N-C PDHs to produce blue oxTMB (λ = 652 nm) and yellow oxOPD (λ = 450 nm) with specific absorption peaks, respectively, as shown in Figure 4b. However, there is no obvious change for the ABTS substrate. The experimental results show that $CoS_{1.035}$/N-C PDHs can catalyze the oxidation of positively charged TMB and uncharged OPD but cannot catalyze the oxidation of negatively charged ABTS, which may be related to the surface charge of $CoS_{1.035}$/N-C PDHs. To verify this hypothesis, the surface zeta potential (ζ) was analyzed by a dynamic light scattering instrument. As shown in Figure 4c, $CoS_{1.035}$/N-C PDHs are negatively charged; thus, they could bond with TMB and OPD by the electrostatic interaction, indicating that the peroxidase-like activity of $CoS_{1.035}$/N-C PDHs demonstrates a certain extent of specificity toward chromogenic substrates. Moreover, compared with Co/N-C PDHs (−14.9 mV), Co_3O_4/N-C PDHs (−11.7 mV), $Co_{0.85}Se$/N-C PDHs (−13.9 mV), and CoTe/N-C PDHs (−11.6 mV), $CoS_{1.035}$/N-C PDHs have the strongest negative charge (−17.3 mV), which explains the optimal peroxidase-like activity among the five catalysts, as shown in Figure S7. As reported in the literature, the most artificial peroxidases are able to catalyze H_2O_2 by generating reactive oxygen species (ROS) like hydroxyl radicals (·OH).[32,33] Therefore, we investigated the ROS in this reaction system by adding the specific radical quencher of hydroxyl radicals (·OH). Phthalic acid (PTA) is a radical scavenger that could react with ·OH to impede the catalytic oxidation of TMB.[34,35] Obviously, there are a blue color and strong absorbance at 652 nm in the test system of $CoS_{1.035}$/N-C + TMB + H_2O_2 (Figure 4d). However, when a certain amount of PTA is added into the above reaction solution, the blue color and absorbance at 652 nm decay

https://doi.org/10.1021/acsomega.1c07264
ACS Omega 2022, 7, 11135−11147

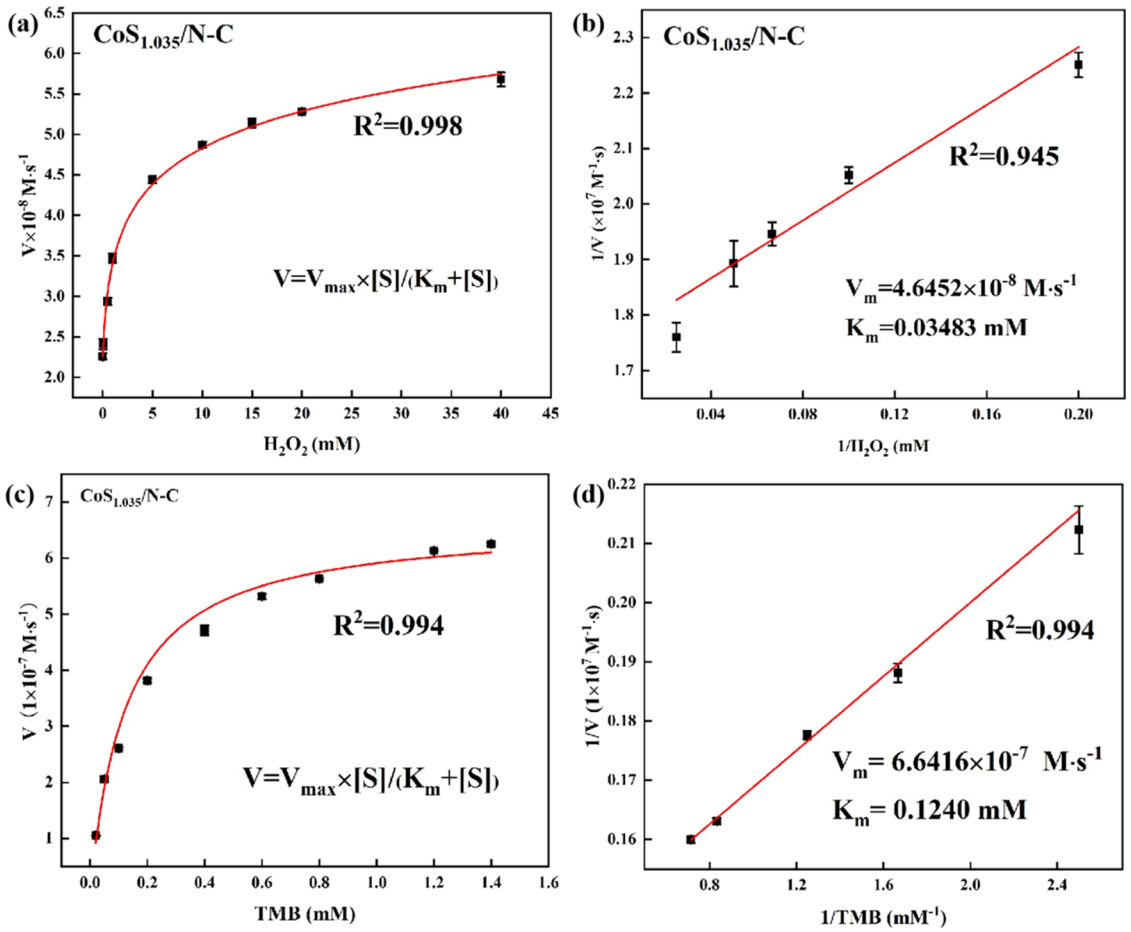

Figure 7. Steady-state kinetic study using the Michaelis−Menten model (a, b) for $CoS_{1.035}$/N-C by varying the concentration of H_2O_2 with a fixed amount of TMB and (c, d) varying the concentration of TMB with a fixed amount of H_2O_2. The error bars represent the standard deviation values of three measurements.

distinctly, confirming that PTA could eliminate the ·OH radicals generated when $CoS_{1.035}$/N-C PDHs exhibited their peroxidase-like activity. Interestingly, a slight oxidation of TMB existed even when the ·OH radicals were eliminated completely by PTA. That is probably because $CoS_{1.035}$/N-C PDHs own a certain extent of oxidase-like activity, which could catalyze the direct oxidation of TMB by the dissolved oxygen. These observations indicate the generation of ·OH in the reaction process that is closely related to the peroxidase-like catalytic mechanism of $CoS_{1.035}$/N-C PDHs, similar to other nanozymes.[36,37]

2.3. Explore the Oxidase-Like Activity of $CoS_{1.035}$/N-C PDHs. Based on the above results, we found that the $CoS_{1.035}$/N-C PDH catalyst also reveals an oxidase-like activity, which could oxidize TMB to produce a blue color with a weak absorbance at 652 nm even in the absence of H_2O_2 (Figure 5a). Notably, the absorbance extremely increases when a certain amount of H_2O_2 is added into the reaction system, implying that the peroxidase-like activity of the $CoS_{1.035}$/N-C PDH catalyst is higher than its oxidase-like activity. In general, the oxidation of TMB without H_2O_2 is driven by dissolved oxygen. Hence, to verify the action of dissolved O_2, the contrast experiments by bubbling inert gas into the system of N_2, air, and O_2 for 30 min were carried out. As displayed in Figure 5b, compared to the air-saturated reaction system, the absorption intensity of oxTMB at 652 nm catalyzed by $CoS_{1.035}$/N-C PDHs exhibits an obvious promotion in the O_2-saturated condition and a significant decrease in the N_2-filled system, illustrating that the catalytic oxidation of TMB demands the participation of dissolved O_2. The dissolved O_2 as the electron acceptor could combine with electrons from TMB to produce ROS ($O_2^{\cdot-}$), which is the real oxidant. In Figure 5c, the oxidase-like activity of $CoS_{1.035}$/N-C PDHs is slightly impeded when the *p*-benzoquinone (PBQ), a scavenger of the superoxide radical ($O_2^{\cdot-}$), is introduced into the reaction system without H_2O_2, suggesting that small doses of $O_2^{\cdot-}$ are produced in the oxidase-like reaction system.

2.4. Catalytic Mechanism of $CoS_{1.035}$/N-C PDHs. The electron paramagnetic resonance (EPR) spectrum in Figure 6a offers more direct evidences. The 5,5-dimethyl-1-pyridine *N*-oxide (DMPO) is selected as the spin capture reagent, which could react with oxygen-centered free radicals, such as ·OH and $O_2^{\cdot-}$, to generate the more stable free radical adducts.[38] Consequently, the production of ·OH and $O_2^{\cdot-}$ was also monitored by incorporating DMPO. As depicted in Figure 6a, the characteristic spectrum of the DMPO/OH adduct with an intensity of 1:2:2:1 can be detected.[39] Likewise, Figure 6a displays the signal of the DMPO/$O_2^{\cdot-}$ adduct with six characteristic peaks.[40] Based on the above results, a possible mechanism for the generation of ·OH and $O_2^{\cdot-}$ by the $CoS_{1.035}$/N-C PDH catalyst with peroxidase- and oxidase-like activities is provided in Figure 6b. In the presence of H_2O_2, the oxidation of TMB is on account of the electron transfer from the nonbonding orbital (NBO) of TMB to the lowest

https://doi.org/10.1021/acsomega.1c07264
ACS Omega 2022, 7, 11135−11147

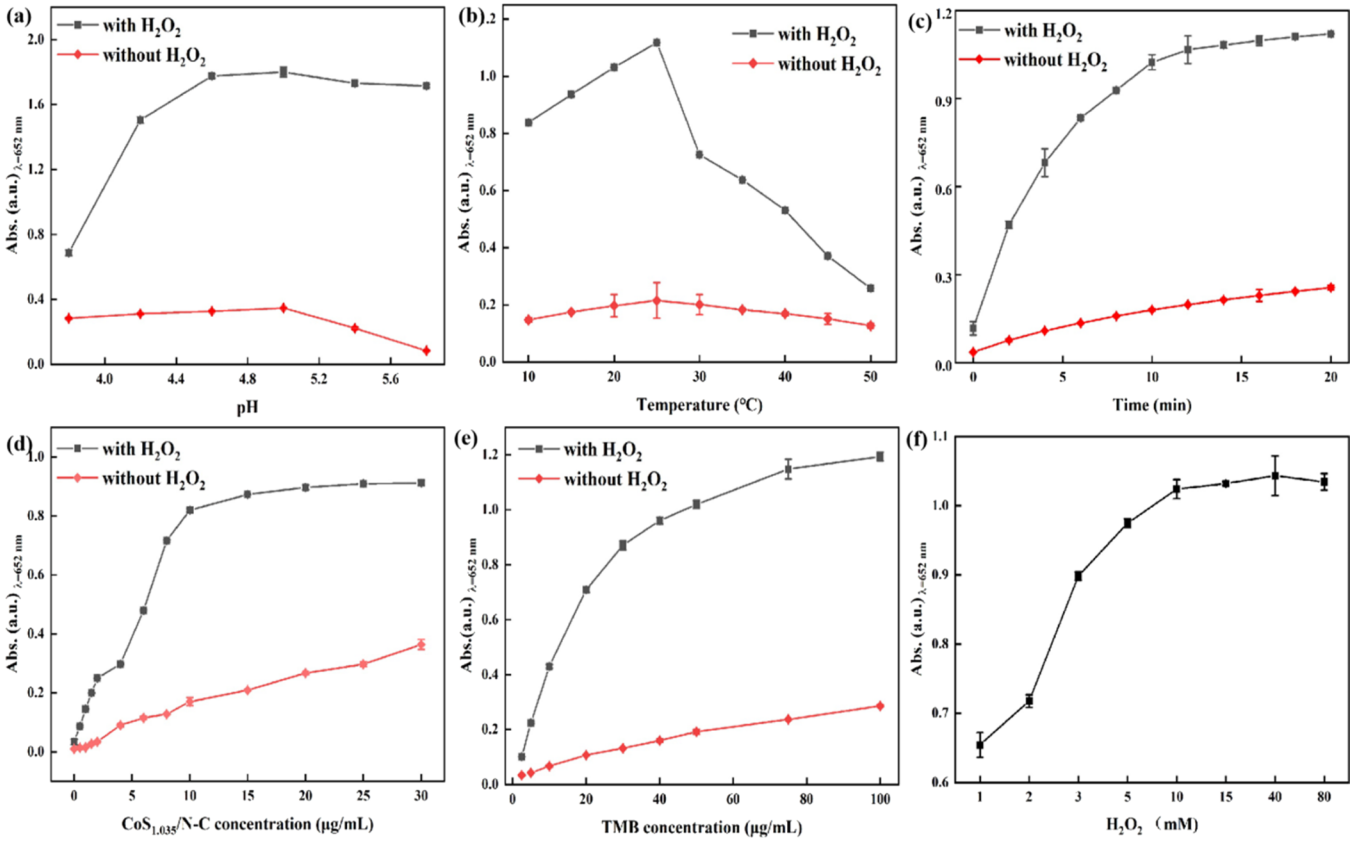

Figure 8. (a) The effect of solution pH on the catalytic activity of $CoS_{1.035}$/N-C. (b) The effect of temperature on the catalytic activity of $CoS_{1.035}$/N-C. (c) The effect of time on the catalytic activity of $CoS_{1.035}$/N-C in the absence and presence of H_2O_2. (d) The effect of $CoS_{1.035}$/N-C concentration on the catalytic activity of $CoS_{1.035}$/N-C. (e) The effect of TMB concentration on the catalytic activity of $CoS_{1.035}$/N-C. (f) The effect of H_2O_2 concentration on the catalytic activity of $CoS_{1.035}$/N-C. The error bars represent the standard deviation values of three measurements.

unoccupied molecular orbital (LUMO) of H_2O_2. In this process, the $CoS_{1.035}$/N-C PDH catalyst receives the lone pair electron from NBO of TMB and then transfers it into the LUMO of H_2O_2, resulting in the breakage of O−O bonds and production of ·OH. Meanwhile, the TMB is catalytically oxidized into oxTMB due to the loss of electrons. In the absence of H_2O_2, the electrons from TMB rapidly transfer to the $CoS_{1.035}$/N-C PDH catalyst, and then the dissolved O_2 absorbed on the surface of the $CoS_{1.035}$/N-C PDH catalyst serves as the electron acceptor, which receives the electrons to form the ROS of $O_2^{\cdot-}$. In parallel, the TMB is catalytically oxidized into oxTMB with the responses of color and absorbance. In summary, the $CoS_{1.035}$/N-C PDH catalyst could disintegrate H_2O_2 and the physically/chemically absorbed O_2 into different ROS species (·OH and $O_2^{\cdot-}$), consequently illustrating the prominent dual-enzyme mimic activities.

2.5. Analysis of Steady-State Kinetic of $CoS_{1.035}$/N-C PDHs. To explore the enzyme-like catalytic properties of $CoS_{1.035}$/N-C PDHs, TMB and H_2O_2 were used as substrates to study the steady-state kinetics of the system by changing one and keeping the other unchanged in the appropriate concentration range. Figure 7a,c shows the steady-state kinetic studies of H_2O_2 (concentration range: 0.1−40 mM) and TMB (concentration range: 0.02−1.4 mM), respectively. Figure 7b,d shows the Michaelis−Menten curves of H_2O_2 and TMB, respectively, which are obtained by fitting the Michaelis−Menten function. Among them, the Michaelis constants K_m and V_m are obtained from the following equation:

$$V_0 = V_m[S]/(K_m + [S])$$

wherein V_m is the maximum reaction rate, V_0 is the initial rate, $[S]$ refers to the substrate (H_2O_2 or TMB) concentration, and K_m is the substrate concentration when the reaction rate reaches half of the maximum reaction rate. The values of V_m and K_m reflect the catalytic activity and affinity of the catalyst with the substrate. The higher the V_m is, the better is the catalytic activity of the catalyst. The smaller the K_m value is, the stronger is the affinity between the catalyst and substrate. According to Figure 7 and Figure S11, the K_m and V_m values of $CoS_{1.035}$/N-C PDHs are listed in Table S3. The K_m value of $CoS_{1.035}$/N-C PDHs with substrate H_2O_2 and TMB is 0.0348 and 0.124 mM, respectively, and the V_m value is 4.645×10^{-8} and 6.642×10^{-7}. As expected, the K_m value of $CoS_{1.035}$/N-C PDHs is lower than that of Co/N-C, Co_3O_4/N-C, $Co_{0.85}Se$/N-C, and CoTe/N-C, while the V_m value of $CoS_{1.035}$/N-C PDHs is higher than their corresponding values (see Table S3). From these experimental results, it is concluded that $CoS_{1.035}$/N-C PDHs have remarkable affinity and catalytic activity. And their catalytic activity is comparable to that of horseradish peroxidase (HRP), as exhibited in Table S3. Consequently, they can be used to replace natural enzymes. Such a high catalytic activity of $CoS_{1.035}$/N-C PDHs might be attributed to the following merits: (1) the high surface area and abundant pores facilitate the rapid diffusion of reaction molecules to the

https://doi.org/10.1021/acsomega.1c07264
ACS Omega 2022, 7, 11135−11147

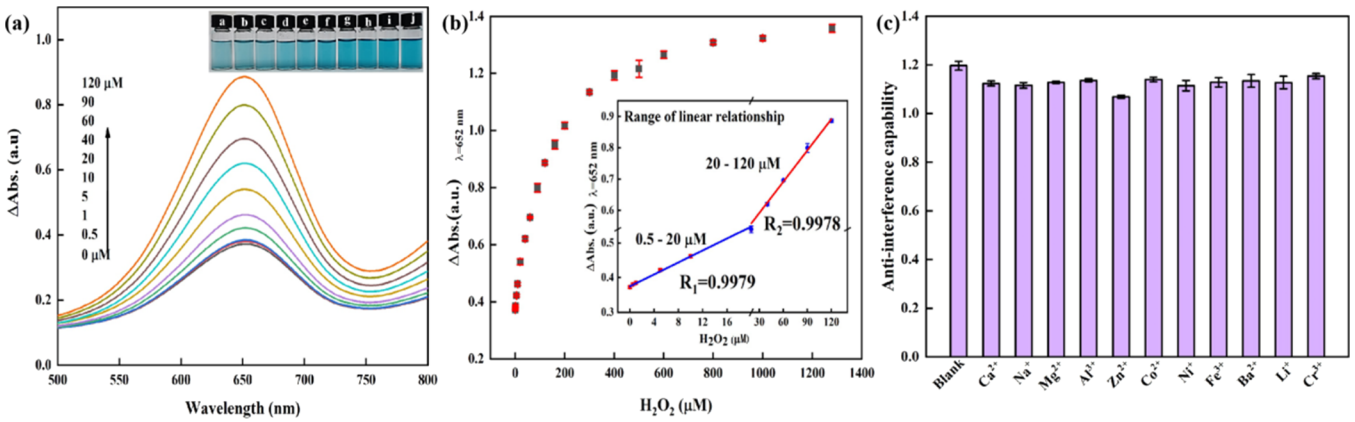

Figure 9. (a) The characteristic spectra of $CoS_{1.035}$/N-C (15 μg/mL) + TMB (50 μg/mL) + HAc-NaAc buffer solution (pH = 5) + different doses of H_2O_2 (from 0 to 120 μM) system at 652 nm. Inset: a color contrast photo of H_2O_2 detection from 0 to 120 mM. (b) A concentration−response curve for the sensitive determination of H_2O_2 under the optimized conditions. Inset: a liner calibration plot for the detection of H_2O_2. The error bars represent the standard deviation of three measurements. (c) Anti-interference of the TMB turn to be blue under the H_2O_2 and $CoS_{1.035}$/N-C with peroxidase mimics. From left to right: blank, Ca^{2+}, Na^{+}, Mg^{2+}, Al^{3+}, Zn^{2+}, Co^{2+}, Ni^{2+}, Fe^{3+}, Ba^{2+}, Li^{+}, and Cr^{3+} (the concentration of the substance in the system: TMB, 50 μg/mL; HAc-NaAc buffer solution, pH 5.0; $CoS_{1.035}$/N-C, 15 μg/mL; H_2O_2, 10 mM; and interference ions, 50 mM).

catalytic active sites, and (2) N-doping could increase the density of the electronic states of carbon, accelerating the interfacial electron transfer between the catalyst and substrates, which promotes H_2O_2/dissolved O_2 to produce ROS with strong oxidation ability. Consequently, $CoS_{1.035}$/N-C PDHs reveal remarkable catalytic performances.

2.6. Optimizing the Reaction Conditions of $CoS_{1.035}$/N-C PDHs. To further master the bifunctional enzyme-like catalytic properties of $CoS_{1.035}$/N-C PDHs, the reaction conditions affecting the activity of $CoS_{1.035}$/N-C PDHs were optimized. Several significant parameters, such as pH, concentration, temperature, and reaction time, were researched to acquire the optimal catalytic activity. As is well known, the pH value has a huge effect on the catalytic activity of natural enzymes. Therefore, we first explored the dependence of pH value on peroxidase-like and oxidase-like activities. From Figure 8a and Figure S12a, it can be concluded that the optimal peroxidase-like activity of $CoS_{1.035}$/N-C PDHs focuses in the pH range of 4.2−5.4. And the satisfactory pH range for oxidase-like activity is determined to be 4.6−5.2, as demonstrated by the more intense colorimetric responses in reaction solutions (inset in Figure S12b). As a result, both peroxidase- and oxidase-like activities could achieve the optimum state at a pH value of 5.0, which is close to the condition (pH = 4.5) of natural HRP. Besides, the catalytic activities display a change tendency of increase first and then decrease as the reaction temperature rises (Figure 8b and Figure S12c,d). And the peroxidase-like reaction system exhibits an activity−temperature relationship similar to that of the oxidase-like reaction system. As such, 25 °C is chosen for the best catalytic performance. According to Figure 8c and Figure S12e,f, the absorbance at 652 nm increases with time and then remains constant after 10 min. In addition, Figure 8d−f and Figure S12g−l show that the absorbance is concentration-dependent. To maximize the enzyme-like catalytic activities, the optimal concentration of $CoS_{1.035}$/N-C PDHs, TMB, and H_2O_2 is also identified as 15 $\mu g \cdot mL^{-1}$, 50 $\mu g \cdot mL^{-1}$, and 10 mM, respectively. Consequently, in the subsequent experiments, the optimized conditions are as follows: $CoS_{1.035}$/N-C PDHs = 15 $\mu g \cdot mL^{-1}$, TMB = 50 $\mu g \cdot mL^{-1}$, H_2O_2 = 10 mM, pH = 5.0, T = 25 °C, and t = 10 min.

Considering the influence of leaching ions on the catalytic activity, the $CoS_{1.035}$/N-C PDHs catalyst was immersed in the above reaction solution under experimental conditions for 25 days, and then the supernatant was collected by centrifugation. Following that, the supernatant was used to catalyze TMB in the presence and absence of H_2O_2. Figure S13a demonstrates that the peroxidase- and oxidase-like catalytic activities are not dependent on the leaching ions; that is to say, the dual-enzyme mimic catalytic activities of $CoS_{1.035}$/N-C PDHs are derived from the nanomaterial itself. What's more, the stability and reproducibility of $CoS_{1.035}$/N-C PDHs were tested by recycling and reusable experiments. After five cycles, the catalytic activity of $CoS_{1.035}$/N-C PDHs still remained at 70.3 and 59.8% of their initial activity, revealing the favorable reproducibility (Figure S13b). Beyond that, the catalytic activities are almost unchanged after preserving in an aqueous solution for 25 days (Figure S13c). The excellent stability is superior to many cobalt-based mimic enzymes, as shown in Table S4. Moreover, no obvious change was found in the XRD data (Figure S14a) and SEM image (Figure S14b) after the stability test, further indicating that $CoS_{1.035}$/N-C PDHs own outstanding long-term stability.

2.7. Determination and Colorimetric Assay of H_2O_2. H_2O_2 is a biomolecule widely used in food, chemistry, environmental conservation, and medical treatment fields. In chemical production, H_2O_2 can be applied to the preparation of fine chemicals. The addition of H_2O_2 in the food process can kill food spoilage bacteria and play a preservative role;[41] in the field of environmental remediation, it is used for environmental pollutant control and wastewater treatment;[42] in medical treatment, H_2O_2 is used for wound treatment, disinfection, and sterilization.[43] In addition, as one of the representative reactive oxygen species, the content of H_2O_2 in the body is also closely related to many diseases, such as Alzheimer's disease,[44] Parkinson's disease,[45] chronic obstructive pulmonary disease (COPO),[46] and cancer.[47] Therefore, it is very critical to construct a fast and sensitive real-time analysis platform of H_2O_2 for environmental protection, food, and

https://doi.org/10.1021/acsomega.1c07264
ACS Omega 2022, 7, 11135−11147

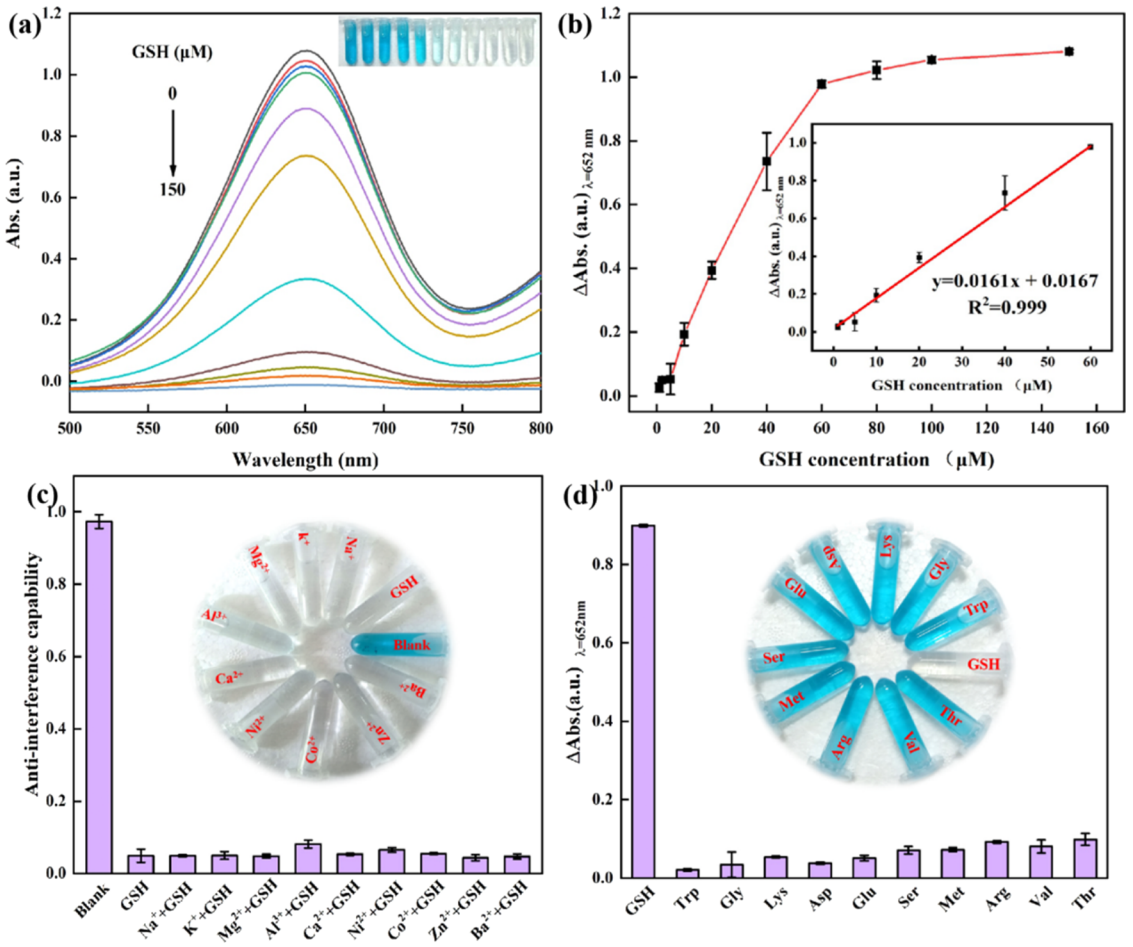

Figure 10. (a) The UV−vis absorption spectrum changes of the mixing solution consisting of TMB (50 μg/mL), $CoS_{1.035}$/N-C catalyst (15 μg/mL), and H_2O_2 (10 mM) in the absence or presence of varied concentrations of GSH. (b) The linear calibration plot for GSH detection. (c) Anti-interference performance of the GSH detection. From left to right: blank, Na^+, K^+, Mg^{2+}, Al^{3+}, Ca^{2+}, Ni^{2+}, Co^{2+}, Zn^{2+}, and Ba^{2+}. The concentration of the substance in the system: TMB, 50 μg/mL; HAc-NaAc buffer solution, pH 5.0; $CoS_{1.035}$/N-C, 15 μg/mL; H_2O_2, 10 mM; GSH, 60 μM; and interference ions, 5 mM. (d) Selectivity of this detection platform for GSH assay. From left to right: GSH, tryptophan, glycine, lysine, aspartic acid, glutamic acid, serine, methionine, arginine, valine, and threonine (the concentration of the substance in the system: TMB, 50 μg/mL; HAc-NaAc buffer solution, pH 5.0; $CoS_{1.035}$/N-C, 15 μg/mL; H_2O_2, 10 mM; GSH, 60 μM; and other amino acids, 60 μM). The error bars represent the standard deviation values of three measurements.

disease diagnosis. Due to the advantages of being visible to the naked eye, fast response, low cost, and simple operation, the colorimetric method for the determination of H_2O_2 has gradually captured people's attention.

Therefore, based on the optimal reaction conditions, a H_2O_2 sensing platform was engineered. Figure 9a is the UV−vis absorption spectrum. When there is no H_2O_2, the absorbance value of the system is the lowest and the blue color of the solution is the lightest (embedded photo (a) in Figure 9a). With the increase of H_2O_2 content, the absorbance value becomes larger and the visual blue becomes darker (embedded graphs (b−j) in Figure 9a). Besides, as illustrated in Figure 9b, in a certain range, the concentration of H_2O_2 has a linear relationship with the absorbance. The linear range of H_2O_2 concentration is 0.5−20 μM (R_1 = 0.9979) and 20−120 μM (R_2 = 0.9978), respectively. The detection limit is 50 nM, which is comparable to or better than that of previous reports (see Table S4). These results show that $CoS_{1.035}$/N-C PDHs with peroxidase-like activity have a wide linear range (0.5−120 μM) and quite low detection limit (50 nM) as a H_2O_2 sensor and can be used for the colorimetric detection of H_2O_2 just by color comparison.

To verify the reliability of the existing method, several common interferences in lakes and tap water were measured, as shown in Figure 9c, namely, Ca^{2+}, Na^+, Mg^{2+}, Al^{3+}, Zn^{2+}, Co^{2+}, Ni^{2+}, Fe^{3+}, Ba^{2+}, Li^+, and Cr^{3+}, which indicated that the proposed method had good anti-interference ability. Additionally, to further confirm the potential application of this method in H_2O_2 detection, the H_2O_2 concentration in labeled real samples was detected. The recoveries were investigated by adding a known amount of the standard H_2O_2 solution to the sample. As shown in Table S5, the average recoveries of H_2O_2 at three spiked levels range from 82.0 to 110.6%. The satisfactory recovery shows that the method has a potential application prospect in the determination of H_2O_2 concentration in lakes and tap water.

2.8. Determination and Colorimetric Assay of GSH.

Glutathione (GSH) is the most abundant tripeptide thiol in eukaryotic cells, and an abnormal GSH level is able to reflect many types of diseases, such as liver injury, cancer, and acquired immune deficiency syndrome.[9] Therefore, it is necessary to establish a simple and reliable detection method of GSH level for disease diagnosis. Considering that GSH is an antioxidant, it can inhibit the oxidation of TMB. The

https://doi.org/10.1021/acsomega.1c07264
ACS Omega 2022, 7, 11135−11147

nanozymes with peroxidase- and oxidase-like activity can be applied to detect such antioxidants.[48,49] So a biosensor is constructed with the $CoS_{1.035}$/N-C PDH nanozyme to realize the visual detection of GSH. As witnessed in Figure 10a, with the increase of GSH concentration, the absorbance at 652 nm gradually declines accompanied with color fading of the reaction system. Figure 10b exhibits the calibration curve for detecting GSH under the optimal reaction conditions. The values of ΔA_{652} ($\Delta A_{652} = A_{blank} - A_{GSH}$) are proportional to GSH concentrations in the linear range of 1−60 μM with a low detection limit of 42 nM ($S/N = 3$). The detection limit based on this method is superior to most limits reported in the literature to date (see Table S6). More importantly, the $CoS_{1.035}$/N-C PDH nanozyme also displays a prominent selectivity and anti-interference ability for detecting GSH. As shown in Figure 10c,d, various types of inorganic metal ions and biological molecules, for instance, K^+, Na^+, Mg^{2+}, Al^{3+}, Ca^{2+}, Ni^{2+}, Co^{2+}, Zn^{2+}, Ba^{2+}, tryptophan, glycine, lysine, aspartic acid, glutamic acid, serine, methionine, arginine, valine, and threonine, are adopted as latent interferences. We found that even if the concentration of the latent interferences is 80 times higher than that of GSH, there is no significant effect on GSH detection. The results indicate the great potential of $CoS_{1.035}$/N-C PDHs to detect the GSH.

3. CONCLUSIONS

In summary, we have successfully designed the $CoS_{1.035}$/N-C PDHs as bifunctional enzyme mimics with superior peroxidase-like and oxidase-like activities using a facile wet chemical method followed by high heat treatment. It can rapidly convert colorless TMB into blue ox-TMB in the presence and absence of H_2O_2. And the catalytic mechanism of $CoS_{1.035}$/N-C PDHs toward the dual-enzyme mimic activities was revealed by investigating the reactive oxygen species. The satisfactory dual-enzyme mimic activities of $CoS_{1.035}$/N-C PDHs are ascribed to the structural advantages, such as the abundant pores, huge exposure surface area, N atom doping, and stable carbon framework. Therefore, the bifunctional platform for the colorimetric detection of H_2O_2 and GSH has been developed, which exhibits a wide linear range and a low detection limit. The present research opens the way for the development of Co-based chalcogenides as dual-enzyme mimics in the fields of biochemical sensing, biomedicine, and environmental monitoring.

4. EXPERIMENTAL SECTION

4.1. Chemicals and Materials. Cobalt nitrate hexahydrate ($Co(NO_3)_2{\cdot}6H_2O$, 99.99%), 2-methylimidazole ($C_4H_6N_2$, 98%), and sulfur sublimed (S, 99.99%) were provided by Chengdu Kelong Chemical Co. Selenium (Se, 99.99%) was obtained from SAAN Chemical Technology Co. Tellurium (Te ,99.99%) was purchased from Shanghai Macklin Biochemical Co., Ltd. Ethyl alcohol (C_2H_5OH, 99.5%, AR), Ltd.Ltd. 3,3′,5,5′-Tetramethylbenzidine dihydrochloride (TMB, 98%) was obtained from Aladdin. Hydrogen peroxide solution (H_2O_2, 30%) was obtained from Chuandong Chemical. In these experiments, all raw materials were not further purified, and deionized (DI) water (18.2 MΩ·cm) was used throughout the experiments.

4.2. Apparatus. The nanomaterials were characterized by different techniques. Field-emission transmission electron microscopy (FETEM, FEI, Tecnai G2 F20, 200 kV) and scanning electron microscopy (FESEM, Hitachi, SU820, 3.0 kV) were used to analyze the micromorphology and surface structure of the as-obtained products. Elemental mapping data were collected by SEM. The crystalline structure and phase purity of the samples were analyzed by X-ray diffraction (XRD) on an XRD-6100 X-ray diffractometer (2 kW, NF, Cu tube) at room temperature. X-ray photoelectron spectroscopy (XPS) data were obtained with an ESCALAB 250 X-ray photoelectron spectrometer (Thermo, USA). Binding energies (BEs) were calibrated by setting the measured BE of C 1s to 284.8 eV. EPR data were collected by an A300-10/12 electron paramagnetic resonance spectrometer (Bruker, Germany). The absorption spectra were measured using a UV-2550 UV−vis spectrophotometer (Shimadzu, Kyoto, Japan).The zeta potential data were obtained by dynamic light scattering (Brookhaven, USA). A dissolved oxygen meter (Beijing, Chiana) was adapted to analyze the content of dissolved oxygen in the system. A high-speed TGL-16M centrifuge (Xiangyi, China) was used in the purification of samples.

4.3. Synthesis of ZIF-67 and Its Derivatives. *4.3.1. Preparation of ZIF-67.* The ZIF-67 dodecahedrons were synthesized by a familiar room-temperature precipitation method.[1] First, 300 mg of $Co(NO_3)_2{\cdot}6H_2O$ was dissolved in 150 mL of CH_3OH to form solution A, and 5 g of 2-methylimidazole ($C_4H_6N_2$) was dissolved in 150 mL of CH_3OH to gain solution B. Then, solution B was rapidly added into solution A under magnetic stirring. Subsequently, the synthetic mixture was stirred for 24 h at room temperature. The final product was centrifuged and washed several times with CH_3OH. Finally, after drying at 60 °C for 12 h, the ZIF-67 dodecahedrons were obtained.

4.3.2. Synthesis of Co/N-C PDHs. The Co/N-C PDHs with the morphology of ZIF-67 were prepared by pyrolyzing the as-obtained ZIF-67 dodecahedrons in a N_2 atmosphere. First, 100 mg of ZIF-67 dodecahedrons was spread in a graphite boat. Then, the graphite boat was placed in a tube furnace; after calcining the graphite boat at 600 °C for 1.5 h under a N_2 atmosphere, the black powder of Co/N-C PDHs was obtained.

4.3.3. Synthesis of Co_3O_4/N-C PDHs. The as-prepared Co/N-C PDHs were first spread in the graphite boat, and then the graphite boat was placed in a tube furnace to calcine for 1.5 h at 600 °C. Afterward, the Co_xO/N-C was obtained.

4.3.4. Synthesis of Co_xM/N-C (M = S, Se, Te) PDHs. First, 50 mg of the as-prepared Co/N-C PDHs and 30 mg of sulfur sublimed/selenium powder/tellurium powder were placed downstream and upstream of the graphite boat, respectively. Then, the graphite boat was transferred to a tube furnace to calcine for 1.5 h at 600 °C at a heating rate of 0.5 °C/min under a N_2 atmosphere. Finally, after natural cooling, the Co_xM/N-C was obtained.

4.4. Evaluation of the Enzyme-Like Activity of $Co_{1.035}S$/N-C PDHs. With TMB as the chromogenic substrate, the peroxidase-mimicking catalytic capacity of $Co_{1.035}S$/N-C PDHs was evaluated. In the presence of H_2O_2, $Co_{1.035}S$/N-C PDHs can rapidly catalyze the oxidation of colorless TMB into blue oxidized TMB. First, the steady-state kinetic study of $Co_{1.035}S$/N-C PDHs was carried out. Then, with the evolution of reaction time, the absorbance of the available reaction system at 652 nm was recorded by a UV-2550 spectrophotometer. Experimental conditions were as follows: $Co_{1.035}S$/N-C PDHs, 15 $\mu g{\cdot}mL^{-1}$; TMB, 50 $\mu g{\cdot}mL^{-1}$; H_2O_2, 10 mM; HAc-NaAc buffer solution, pH = 5; and reaction time, 10 min. After 10 min of reaction, the absorbance of the system reached

https://doi.org/10.1021/acsomega.1c07264
ACS Omega 2022, 7, 11135−11147

a stable value. Hence, this result reveals that the optimized reaction time is 10 min. Following that, under the optimized time, other factors affecting the peroxidase-like capacity of $Co_{1.035}S$/N-C PDHs such as pH and substrate concentration (including TMB and H_2O_2) were elaborately investigated. In addition, the affinity between $Co_{1.035}S$/N-C PDHs and the substrate was investigated by calculating K_m. Keeping the content of catalysts constant and altering the concentration of substrate, the reaction kinetics of the system were recorded by a UV-2550 spectraphotometer. Finally, the Lineweaver−Burk plot was applied to fit the obtained curve and analyze data.

■ ASSOCIATED CONTENT

Supporting Information

The Supporting Information is available free of charge at https://pubs.acs.org/doi/10.1021/acsomega.1c07264.

SEM, XRD, TG, UV−vis, elemental mapping images, BET, Raman, and ICP data (PDF)

■ AUTHOR INFORMATION

Corresponding Authors

Li Liu − *Chongqing Key Laboratory of Green Synthesis and Applications, College of Chemistry, Chongqing Normal University, Chongqing 401331, China;* orcid.org/0000-0002-9069-2797; Email: liliu1208@163.com

Yanhua Hou − *Chongqing Engineering Research Center of Pharmaceutical Sciences, Chongqing Medical and Pharmaceutical College, Chongqing 401331, China;* Email: hyh9785@163.com

Wensheng Fu − *Chongqing Key Laboratory of Green Synthesis and Applications, College of Chemistry, Chongqing Normal University, Chongqing 401331, China;* orcid.org/0000-0002-8969-3856; Email: fuwensheng@cqnu.edu.cn

Authors

Tao Chen − *Chongqing Key Laboratory of Green Synthesis and Applications, College of Chemistry, Chongqing Normal University, Chongqing 401331, China*

Yuanhong Min − *Chongqing Key Laboratory of Green Synthesis and Applications, College of Chemistry, Chongqing Normal University, Chongqing 401331, China*

Xiao Yang − *Chongqing Key Laboratory of Green Synthesis and Applications, College of Chemistry, Chongqing Normal University, Chongqing 401331, China*

Hao Gong − *Chongqing Key Laboratory of Green Synthesis and Applications, College of Chemistry, Chongqing Normal University, Chongqing 401331, China*

Xiaoying Tian − *Chongqing Key Laboratory of Green Synthesis and Applications, College of Chemistry, Chongqing Normal University, Chongqing 401331, China*

Complete contact information is available at: https://pubs.acs.org/10.1021/acsomega.1c07264

Author Contributions

§T.C. and Y.M. contributed equally.

Notes

The authors declare no competing financial interest.

■ ACKNOWLEDGMENTS

This work was supported by the Chongqing Research Program of Basic Research and Frontier Technology (cstc2019jcyj-msxmX0523), Science and Technology Research Program of Chongqing Municipal Education Commission (KJZD-K201900503), Achievement Transfer Program of Institutions of Higher Education in Chongqing (KJZH17112), Chongqing Research Program of Basic Research and Frontier Technology (cstc2018jcyjAX0580), Innovation and Entrepreneurship Team of Inorganic Optoelectronic Functional Materials for Chongqing Yingcai (cstc2021ycjh-bgzxm0131), Chongqing Innovation Research Group Project (CXQT21015), Doctor Start/Talent Introduction Program of Chongqing Normal University (02060404/2020009000321), and the fund of Chongqing Normal University Graduate Research Innovation Project (YKC20044). W. Fu was sponsored by the Chongqing Talent Program (Leading talent).

■ REFERENCES

(1) Kotov, N. A. Inorganic Nanoparticles as Protein Mimics. *Science* **2010**, *330*, 188.

(2) Breaker, R. R. DNA Enzymes. *Nat. Biotechnol.* **1997**, *15*, 427−431.

(3) Wei, H.; Gao, L.; Fan, K.; Liu, J.; He, J.; Qu, X.; Dong, S.; Wang, E.; Yan, X. Nanozymes: A clear definition with fuzzy edges. *Nano Today* **2021**, *40*, 101269.

(4) Wei, H.; Wang, E. Nanomaterials with Enzyme-like Characteristics (Nanozymes): Next-generation Artificial Enzymes. *Chem. Soc. Rev.* **2013**, *42*, 6060−6093.

(5) Wu, J.; Wang, X.; Wang, Q.; Lou, Z.; Li, S.; Zhu, Y.; Qin, L.; Wei, H. Nanomaterials with Enzyme-like Characteristics (nanozymes): Next-generation Artificial Enzymes (II). *Chem.Soc. Rev.* **2019**, *48*, 1004−1076.

(6) Gao, L.; Zhuang, J.; Nie, L.; Zhang, J.; Zhang, Y.; Gu, N.; Wang, T.; Feng, J.; Yang, D.; Perrett, S.; et al. Intrinsic Peroxidase-Like Activity of Ferromagnetic Nanoparticles. *Nat. Nanotechnol.* **2007**, *2*, 577−583.

(7) Xi, Z.; Cheng, X.; Gao, Z.; Wang, M.; Cai, T.; Muzzio, M.; Davidson, E.; Chen, O.; Jung, Y.; Sun, S.; et al. Strain Effect in Palladium Nanostructures as Nanozymes. *Nano Lett.* **2020**, *20*, 272−277.

(8) Zeng, L.; Cheng, H.; Dai, Y.; Su, Z.; Wang, C.; Lei, L.; Lin, D.; Li, X.; Chen, H.; Fan, K.; et al. In Vivo Regenerable Cerium Oxide Nanozyme-Loaded pH/H2O2-Responsive Nanovesicle for Tumor-Targeted Photothermal and Photodynamic Therapies. *ACS Appl. Mater. Interfaces* **2021**, *13*, 233−244.

(9) Song, C.; Ding, W.; Zhao, W.; Liu, H.; Wang, J.; Yao, Y.; Yao, C. High peroxidase-like activity realized by facile synthesis of FeS_2 nanoparticles for sensitive colorimetric detection of H_2O_2 and glutathione. *Biosens. Bioelectron.* **2020**, *151*, 111983.

(10) Ling, Y.; Cao, T.; Liu, L.; Xu, J.; Zheng, J.; Li, J.; Zhang, M. Fabrication of noble metal nanoparticles decorated on one dimensional hierarchical polypyrrole@MoS_2 microtubes. *J. Mater. Chem. B* **2020**, *8*, 7801−7811.

(11) Peng, H.; Zheng, J.; Zhang, B.; Xu, J.; Zhang, M. Fe doped MoS_2/polypyrrole microtubes towards efficient peroxidase mimicking and colorimetric sensing application. *Dalton Trans.* **2021**, *50*, 15380−15388.

(12) Song, Y.; Qu, K.; Zhao, C.; Ren, J.; Qu, X. Graphene Oxide: Intrinsic Peroxidase Catalytic Activity and Its Application to Glucose Detection. *Adv. Mater.* **2010**, *22*, 2206−2210.

(13) Wang, J.; Hu, Y.; Zhou, Q.; Hu, L.; Fu, W.; Wang, Y. Peroxidase-like Activity of Metal−Organic Framework [Cu(PDA)-(DMF)] and Its Application for Colorimetric Detection of Dopamine. *ACS Appl. Mater. Interfaces* **2019**, *11*, 44466−44473.

(14) Niu, X.; Shi, Q.; Zhu, W.; Liu, D.; Tian, H.; Fu, S.; Cheng, N.; Li, S.; Smith, J. N.; Du, D.; et al. Unprecedented Peroxidase-mimicking Activity of Single-atom Nanozyme with Atomically Dispersed Fe−Nx Moieties Hosted by MOF Derived Porous Carbon. *Biosens. Bioelectron.* **2019**, *142*, 111495.

(15) Liu, B.; Liu, J. Surface Modification of Nanozymes. *Nano Res.* **2017**, *10*, 1125−1148.
(16) Wang, H.; Wan, K.; Shi, X. Recent Advances in Nanozyme Research. *Adv. Mater.* **2019**, *31*, 1805368.
(17) Jiang, D.; Ni, D.; Rosenkrans, Z. T.; Huang, P.; Yan, X.; Cai, W. Nanozyme: New Horizons for Responsive Biomedical Applications. *Chem. Soc. Rev.* **2019**, *48*, 3683−3704.
(18) Huang, Y.; Ren, J.; Qu, X. Nanozymes: Classification, Catalytic Mechanisms, Activity Regulation, and Applications. *Chem. Rev.* **2019**, *119*, 4357−4412.
(19) Zhou, Y.; Liu, B.; Yang, R.; Liu, J. Filling in the Gaps between Nanozymes and Enzymes: Challenges and Opportunities. *Bioconjugate Chem.* **2017**, *28*, 2903−2909.
(20) Zheng, J.; Song, D.; Chen, H.; Xu, J.; Alharbi, N.; Hayat, T.; Zhang, M. Enhanced peroxidase-like activity of hierarchical MoS_2-decorated N-doped carbon nanotubes with synergetic effect for colorimetric detection of H_2O_2 and ascorbic acid. *Chin. Chem. Lett.* **2019**, *31*, 1109−1113.
(21) Yang, L.; Jin, Z.; Zheng, J.; Zhang, B.; Xu, J.; Yin, X.-B.; Zhang, M. In Situ Construction of Co-MoS_2/Pd Nanosheets on Polypyrrole-Derived Nitrogen-Doped Carbon Microtubes as Multifunctional Catalysts with Enhanced Catalytic Performance. *Inorg. Chem.* **2022**, *61*, 542−553.
(22) Xia, W.; Zhang, P.; Fu, W.; Hu, L.; Wang, Y. Aggregation/dispersion-mediated peroxidase-like activity of MoS_2 quantum dots for colorimetric pyrophosphate detection. *Chem. Commun.* **2019**, *55*, 2039−2042.
(23) He, W.; Jia, H.; Li, X.; Lei, Y.; Li, J.; Zhao, H.; Mi, L.; Zhang, L.; Zheng, Z. Understanding the formation of CuS concave superstructures with peroxidase-like activity. *Nanoscale* **2012**, *4*, 3501−3506.
(24) Zhu, J.; Peng, X.; Nie, W.; Wang, Y.; Gao, J.; Wen, W.; Selvaraj, J. N.; Zhang, X.; Wang, S. Hollow copper sulfide nanocubes as multifunctional nanozymes for colorimetric detection of dopamine and electrochemical detection of glucose. *Biosens. Bioelectron.* **2019**, *141*, 111450.
(25) Jamil, S.; Nasir, M.; Ali, Y.; Nadeem, S.; Rashid, S.; Javed, M. Y.; Hayat, A. Cr_2O_3−TiO_2-Modified Filter Paper-Based Portable Nanosensors for Optical and Colorimetric Detection of Hydrogen Peroxide. *ACS Omega* **2021**, *6*, 23368−23377.
(26) Xiao, D.; Li, Q.; Zhang, H.; Ma, Y.; Lu, C.; Chen, C.; Liu, Y.; Yuan, S. A Sulfur Host Based on Cobalt−graphitic Carbon Nanocages for High Performance Lithium−sulfur Batteries. *J. Mater. Chem. A* **2017**, *5*, 24901−24908.
(27) Guo, S.; Zhang, S.; Wu, L.; Sun, S. Co/CoO Nanoparticles Assembled on Graphene for Electrochemical Reduction of Oxygen. *Angew. Chem., Int. Ed.* **2012**, *51*, 11770−11773.
(28) Jian, S.-L.; Hsiao, L.-Y.; Yeh, M.-H.; Ho, K.-C. Designing A Carbon Nanotubes-interconnected ZIF-derived Cobalt Sulfide Hybrid Nanocage for Supercapacitors. *J. Mater. Chem. A* **2019**, *7*, 1479−1490.
(29) Miao, W.; Zhang, Y.; Li, H.; Zhang, Z.; Li, L.; Yu, Z.; Zhang, W. ZIF-8/ZIF-67-derived 3D Amorphous Carbon-encapsulated CoS/NCNTs Supported on CoS-coated Carbon Nanofibers as An Advanced Potassium-ion Battery Anode. *J. Mater. Chem. A* **2019**, *7*, 5504−5512.
(30) Qiu, X.; Yu, Y.; Peng, Z.; Asif, M.; Wang, Z.; Jiang, L.; Wang, W.; Xu, Z.; Wang, H.; Liu, H. Cobalt Sulfides Nanoparticles Encapsulated in N,S Co-doped Carbon Substrate for Highly Efficient Oxygen Reduction. *J. Alloys Compd.* **2020**, *815*, 152457.
(31) Zheng, F.; Yang, Y.; Chen, Q. High Lithium Anodic Performance of Highly Nitrogen-doped Porous Carbon Prepared from A Metal-organic Framework. *Nat. Commun.* **2014**, *5*, 5261.
(32) Jiang, Z.; Li, H.; Ai, R.; Deng, Y.; He, Y. Electrostatic-driven coordination interaction enables high specificity of UO_2^{2+} peroxidase mimic for visual colorimetric detection of UO_2^{2+}. *ACS Sustainable Chem. Eng.* **2020**, *8*, 11630−11637.
(33) An, Q.; Sun, C.; Li, D.; Xu, K.; Guo, J.; Wang, C. Peroxidase-like activity of Fe_3O_4@carbon nanoparticles enhances ascorbic acid-induced oxidative stress and selective damage to PC-3 prostate cancer cells. *ACS Appl. Mater. Interfaces* **2013**, *5*, 13248−13257.
(34) Lu, W.; Shu, J.; Wang, Z.; Huang, N.; Song, W. The intrinsic oxidase-like activity of Ag_2O nanoparticles and its application for colorimetric detection of sulfite. *Mater. Lett.* **2015**, *154*, 33−36.
(35) Song, N.; Ma, F.; Zhu, Y.; Chen, S.; Wang, C.; Lu, X. Fe_3C/Nitrogen-Doped Carbon Nanofibers as Highly Efficient Biocatalyst with Oxidase-Mimicking Activity for Colorimetric Sensing. *ACS Sustainable Chem. Eng.* **2018**, *6*, 16766−16776.
(36) Luo, W.; Li, Y.-S.; Yuan, J.; Zhu, L.; Liu, Z.; Tang, H.; Liu, S. Ultrasensitive fluorometric determination of hydrogen peroxide and glucose by using multiferroic $BiFeO_3$ nanoparticles as a catalyst. *Talanta* **2010**, *81*, 901−907.
(37) Shi, Y.; Su, P.; Wang, Y.; Yang, Y. Fe_3O_4 peroxidase mimetics as a general strategy for the fluorescent detection of H_2O_2-involved systems. *Talanta* **2014**, *130*, 259−264.
(38) Courtney Colleen, M.; Goodman Samuel, M.; Nagy Toni, A.; Levy, M.; Bhusal, P.; Madinger Nancy, E.; Detweiler Corrella, S.; Nagpal, P.; Chatterjee, A. Potentiating antibiotics in drug-resistant clinical isolates via stimuli-activated superoxide generation. *Sci. Adv.* **2007**, *3*, No. e1701776.
(39) Singh, N.; Savanur, M. A.; Srivastava, S.; D'Silva, P.; Mugesh, G. A Redox Modulatory Mn_3O_4 Nanozyme with Multi-Enzyme Activity Provides Efficient Cytoprotection to Human Cells in a Parkinson's Disease Model. *Angew. Chem., Int. Ed.* **2017**, *56*, 14267−14271.
(40) Su, W.; Chen, J.; Wu, L.; Wang, X.; Wang, X.; Fu, X. Visible light photocatalysis on praseodymium(III)-nitrate-modified TiO_2 prepared by an ultrasound method. *Appl. Catal., B* **2008**, *77*, 264−271.
(41) Toledo, R. T.; Escher, F. E.; Ayres, J. C. Sporicidal Properties of Hydrogen Peroxide Against Food Spoilage Organisms. *Appl. Microbiol.* **1973**, *26*, 592.
(42) Glaze, W. H.; Kang, J.-W.; Chapin, D. H. The Chemistry of Water Treatment Processes Involving Ozone, Hydrogen Peroxide and Ultraviolet Radiation. *Ozone: Sci. Eng.* **1987**, *9*, 335−352.
(43) Kanta, J. The Role of Hydrogen Peroxide and Other Reactive Oxygen Species in Wound Healing. *Acta Med.* **2011**, *54*, 97−101.
(44) Huang, X.; Atwood, C. S.; Hartshorn, M. A.; Multhaup, G.; Goldstein, L. E.; Scarpa, R. C.; Cuajungco, M. P.; Gray, D. N.; Lim, J.; Moir, R. D.; et al. The Aβ Peptide of Alzheimer's Disease Directly Produces Hydrogen Peroxide through Metal Ion Reduction. *Biochemistry* **1999**, *38*, 7609−7616.
(45) Tabner, B. J.; Turnbull, S.; El-Agnaf, O. M. A.; Allsop, D. Formation of Hydrogen Peroxide and Hydroxyl Radicals from Aβ and α-synuclein as A Possible Mechanism of Cell Death in Alzheimer's Disease and Parkinson's Disease. *Free Radical Biol. Med.* **2002**, *32*, 1076−1083.
(46) Dekhuijzen, P. N.; Aben, K. K.; Dekker, I.; Aarts, L. P.; Wielders, P. L.; van Herwaarden, C. L.; Bast, A. Increased Exhalation of Hydrogen Peroxide in Patients with Stable and Unstable Chronic Obstructive Pulmonary Disease. *Am. J. Respir. Crit. Care Med.* **1996**, *154*, 813−816.
(47) DeSesso, J. M.; Lavin, A. L.; Hsia, S. M.; Mavis, R. D. Assessment of the Carcinogenicity Associated with Oral Exposures to Hydrogen Peroxide. *Food Chem. Toxicol.* **2000**, *38*, 1021−1041.
(48) Jia, H.; Yang, D.; Han, X.; Cai, J.; Liu, H.; He, W. Peroxidase-like activity of the Co_3O_4 nanoparticles used for biodetection and evaluation of antioxidant behavior. *Nanoscale* **2016**, *8*, 5938−5945.
(49) Zhang, X.; Han, G.; Zhang, R.; Huang, Z.; Shen, H.; Su, P.; Song, J.; Yang, Y. $Co_2V_2O_7$ Particles with Intrinsic Multienzyme Mimetic Activities as an Effective Bioplatform for Ultrasensitive Fluorometric and Colorimetric Biosensing. *ACS Appl. Bio Mater.* **2020**, *3*, 1469−1480.

https://doi.org/10.1021/acsomega.1c07264
ACS Omega 2022, 7, 11135−11147